Chinese Chemical Letters 36 (2025) 109970

Contents lists available at ScienceDirect

Chinese Chemical Letters

journal homepage: www.elsevier.com/locate/cclet

Carbon bridge effects regulate TiO_2–acrylate fluoroboron coatings for efficient marine antifouling

Jiatong Li[a,b,1], Linlin Zhang[a,b,1], Peng Huang[a,b,*], Chengjun Ge[a,b,*]

[a] Key Laboratory of Agro-Forestry Environmental Processes and Ecological Regulation, School of Environmental Science and Engineering, Hainan University, Haikou 570228, China
[b] Haikou Key Laboratory of Environmental Toxicology (Hainan University), Haikou 570228, China

ARTICLE INFO

Article history:
Received 23 January 2024
Revised 18 April 2024
Accepted 7 May 2024
Available online 8 May 2024

Keywords:
Acrylate fluoroboron
TiO_2
Marine antifouling
Carbon bridge
Synergy antifouling

ABSTRACT

Synergy strategy of photocatalysts and polymer resins are promising technology for marine antifouling. However, it is still a main challenge to obtain a green, safe, and efficient antifouling coatings. Herein, carbon (graphene or CNT) modified TiO_2 photocatalyst was synthesized *via* hydrothermal and annealing process and has successfully applied in acrylate fluoroboron polymer (ABFP) composite coating. Morphology and chemical composition were detailed characterized. The graphene or CNT acted as a bridge with supplemental spatial structures (petal gaps, entanglement) and new functional groups (C–O, C–Ti–O, *etc.*) on TiO_2 particle. Carbon nanotube (CNT) modified TiO_2-ABFP coatings (BTCP) achieved excellent antibacterial and anti-diatom adhesion rate of 89.3%–96.70% and 99.00%–99.50%, which was 1.84–4.94-fold more than that of the single ABFP. CNT or graphene served as electronic bridges was considered as the crucial mechanism, which significantly improved the light absorption range and capacity, conductivity, and photoelectric response of TiO_2, and further accelerated the generation and transfer of free radicals to the surface of BTCP or FTGP. Moreover, the improvement of catalyst activity synergizes with the smooth surface, hydrophilicity, and slow hydrolysis of composite coatings, achieved long-term and efficient antifouling performance. This work provides a new insight into the modification of TiO_2 and antifouling mechanism of polymer coating.

Marine biofouling often occurring on ship hulls or subsea equipment, which significantly increase fossil energy consumption and threatened ecological environmental safety [1–3]. Antifouling coatings are considered one of the most effective and feasible methods to address biofouling issues [4]. Traditional antifouling coatings consist of a large amount of toxic active chemicals, such as organotin [5,6], DDT [7], silver [8], cuprous oxide [9]. These coatings are gradually prohibited by governments around the world due to the high cost and indiscriminately toxic to marine organisms [4,10,11]. Although non-toxic antifouling coatings have been developed, such as siloxane-based coatings [12], bioinspired coatings [13], zwitterionic compounds [14], and fluorinated polymers [15]. In particular, fluorinated polymers coatings stand out in current research due to their good light transmittance, high stability (radiation, heat and pH tolerance), easy synthesis, economy and non-toxic properties [16,17]. However, the highly hydrophobic surface, low viscosity and insufficient long-term effectiveness of fluorinated polymers coatings make it difficult to achieve the expected performance in practical commercial applications [3,18,19]. Literatures indicate that introducing organic boron is also effective in improving the hydrophobicity of fluoropolymers benefit by the special functional groups and properties of boron source [20,21]. Particularly, acrylate fluoroboron polymer (ABFP) has received widespread attention due to its unique fluoroboron side chains and non-toxic. Li *et al.* prepared self-healing antifouling coatings (acrylate boron fluorinated polymer films) through ultrasonic mixing of perfluoropolyether (PFPE) lubricant with ABFP [22]. However, these coatings are usually designed based on a component with one property (antifouling chemicals, surface morphology, hydrophobicity, surface energy, *etc.*) and are unlikely to maintain both eco-friendly and high efficiently in harsh marine environments [23,24].

Photocatalysis is an important representative of utilizing natural energy, opening another direction for the design of efficient and non-toxic antifouling coatings [25,26]. Titanium dioxide (TiO_2) is

* Corresponding authors at: Key Laboratory of Agro-Forestry Environmental Processes and Ecological Regulation, School of Environmental Science and Engineering, Hainan University, Haikou 570228, China.
E-mail addresses: huangpeng207@hainanu.edu.cn (P. Huang), cjge3007@163.com (C. Ge).
[1] These authors contributed equally in this work.

https://doi.org/10.1016/j.cclet.2024.109970
1001-8417/

undoubtedly the most representative and widely applied photocatalyst due to the chemical stable, high catalytic activity, low price, non-toxic and eco-friendly [27,28]. TiO_2 has become an indispensable research object in hydrogen reduction [29], carbon dioxide reduction [30], water decomposition [31], and solar cells [32], while the research on marine antifouling coating and pollutants removal is still unsatisfactory. On the one hand, the single TiO_2 has a short absorption range of sunlight (<387 nm), and a large amount of visible light energy cannot be effectively utilized [33,34]. On the other hand, the rapid recombination of electron-hole pairs restrict the photocatalytic efficiency and reduces the available distance of active species ($\sim 10^{-9}$ s survival time for $^{\bullet}OH$) for the single TiO_2 [30]. In addition, the destruction of non-targeted organism and secondary pollution are highly likely to occurred because of the active radicals generated by TiO_2-light system usually attack organisms and pollutants without selectivity [33]. Consequently, improving the visible light utilization efficiency and expanding the application in antifouling of TiO_2 remains an important challenge. Both graphene and carbon nanotubes (CNT) have excellent charge transport performance, stable mechanical properties, rich oxygen-containing functional groups, and diverse surface chemical properties, and become a powerful helper for TiO_2 in photocatalysis [35,36]. Literatures point out that graphene or CNT can significantly improve the adsorption efficiency, separation efficiency of photo generated carriers, and photocatalytic efficiency of carbon-TiO_2 composite materials in the photocatalytic process [36–38]. Additional CNT or graphene can significantly improve the mechanical strength and stability of organic coatings [39]. The regulatory effect and the application of carbon-modified TiO_2 to enhance the antifouling performance of coatings is worth expecting. Unfortunately, related research is still insufficient, particularly in the appropriate ratio of antifouling coatings to catalysts and the photocatalytic mechanism mediated by coatings.

Tremendous progress can be expected in the marine antifouling if a versatile, long-term effectiveness and eco-friendly coating is designed or fabricated with TiO_2 and ABFP. Herein, we synthesized series of antifouling coatings with ABFP and carbon-modified TiO_2 photocatalyst, as well as optimized preparation parameters. Through detailed characterization, the carbon bridge structure and formation mechanism between carbon-modified TiO_2 and ABFP were revealed. Moreover, *Escherichia coli* (Gram-negative, *E. coli*), *Staphylococcus aureus* (Gram-positive, *S. aureus*), *Nitzschia closterium f.minutissima.* (*NC*) and *Amphora* sp. (*HA*) were selected as typically marine bacteria and algae, respectively, to evaluated the antifouling performance of composite coatings in artificial seawater. Finally, the synergistic antifouling mechanism was proposed that the graphene or CNT acted as electronic bridge efficient mediated the antifouling process of photocatalytic, smooth surface and slow hydrolysis.

Four typically TiO_2 based photocatalyst, including flower-like TiO_2 (FT), graphene modified flower-like TiO_2 (FTG), oxygen enriched TiO_2 (BT) and CNT modified oxygen enriched TiO_2 (BTC) and corresponding ABFP antifouling coatings were synthesis as steps of Fig. 1a. Detailed preparation steps and chemical reagents were shown in Texts S1-S4 (Supporting information). And the characterization methods and batch experiments for antibacterial or antidiatom adhesion performance and mechanism exploration were present in Texts S5-S7 (Supporting information).

Scanning electron microscopy (SEM) images in Figs. 1b and f revealed that FTG and BTC maintain a relatively complete flower-like particle structure. The dispersibility of FTG and BTC were significantly higher than that of FT and BT, which could be attributed to the barrier effect between graphene or CNT and TiO_2 particles (Fig. S2 in Supporting information). Moreover, FTG had a larger particle diameter (4.3 μm) and abundant flocculent petals (Fig. 1b) than BTC (2.2 μm), which was attributed to the layered structure

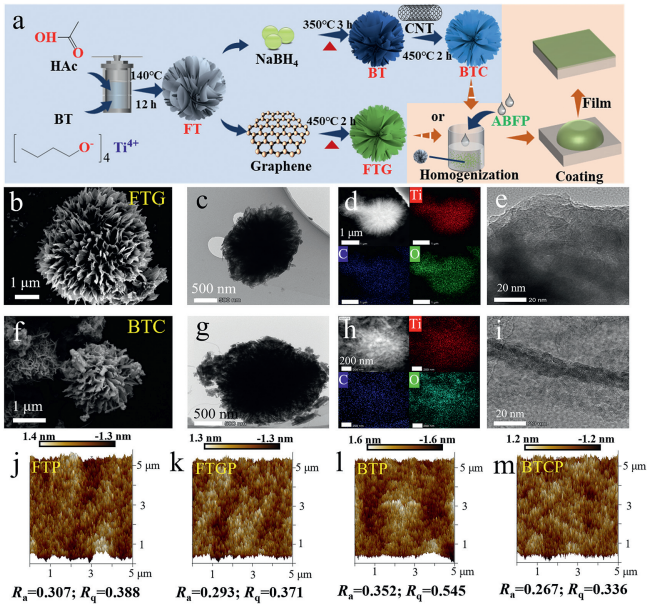

Fig. 1. (a) Schematic diagram of the synthesis of FT, BT, FTG and BTC and corresponding antifouling coating. (b, f) SEM, (c, g) TEM, (d, h) EDS and (e, i) HRTEM image of FTG and BTC, respectively. AFM images and corresponding R_a and R_q values of (j) FTP, (k) FTGP, (l) BTP and (m) BTCP. FT and BT were the TiO_2 samples without added carbon material; FTG and BTC were the samples with 3 wt% addition of graphene and CNT in FT and BT; FTP, FTGP, BTP and BTCP were obtained with 5 wt% corresponding photocatalyst in ABFP coating, respectively. similarly hereinafter.

of graphene and annealing treatment further keep and expand the petal structure. Transmission electron microscope (TEM) results suggested that scattered graphene layers adhering to the petals of TiO_2 particles (Fig. 1c), and the distribution of Ti, C and O elements in the energy dispersive spectrometer (EDS) images showed good consistency (Fig. 1d), indicating that graphene entered the interior of particles. Interestingly, a relatively compact spherical particle was observed in BTC, which may be attributed to the 3 wt% CNT addition and linear CNT wrapped around the petal of TiO_2 (Figs. 1f and g). The uniform C elements distribution in BTC also confirmed this binding of CNT and TiO_2 (Fig. 1h). FT and BT also had obvious flower-like particle structure, but TiO_2 particle in BT exhibits more irregular shape, thin and slender petal structures on particle surface, which might be related to the reduction of $NaBH_4$ (Fig. S3 in Supporting information). High resolution TEM (HRTEM) revealed that amorphous structure was the main form on the interface between graphene or CNT and TiO_2, indicating that graphene or CNT undergoes chemical fusion (bonding) with TiO_2 rather than simple adsorption (Figs. 1e and i). Therefore, we inferred that the graphene or CNT on the surface of FTG or BTC may provide favorable condition for binding to ABFP.

Additionally, atomic force microscopy (AFM) was used to observe the surface morphology and the effect of TiO_2 on the surface roughness of the antifouling coatings. The results of 2D plane (Fig. S4 in Supporting information) and 3D stereogram (Figs. 1j–m) showed that FTP and BTP had more obvious gullies, and the highest (lowest) points on the surface was greater (less) than that of FTGP and BTCP. The R_a or R_q values of four antifouling coatings had the similar orders, as follow: BTCP < FTGP < FTP < BTP. This indicated that the addition of graphene or CNT was favored to integrate ABFP into TiO_2 particles, which might be ascribed to the abundant petal initial structure and functional groups on graphene or CNT of FTG or BTC. Specially, BTCP had lowest R_a (0.267) and R_q (0.336) values, which represented a flatter and smoother surface than other coatings. Silva *et al.* had pointed out that the carbon material on the surface of TiO_2 could improve the adsorp-

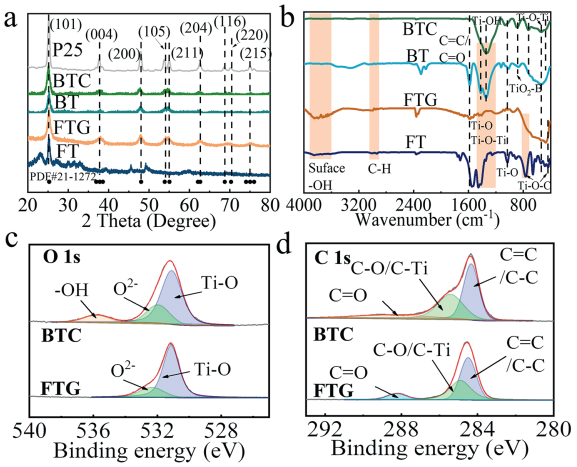

Fig. 2. (a) XRD and (b) FTIR spectra of FT, FTG, BT and BTC. The (c) O 1s and (d) C 1s spectra of FTG and BTC.

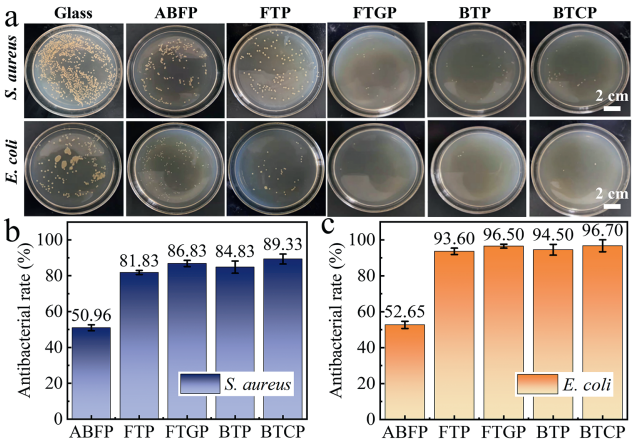

Fig. 3. (a) Antibacterial digital images and (b, c) the antibacterial rate for different coatings.

tion capacity [40]. Therefore, graphene (CNT) on FTG (BTC) surface may act as a carbon bridge through spatial position and functional groups attraction effect and enhance the bonding performance with ABFP.

X-ray diffraction (XRD) results were present in Fig. 2a. Obviously, several high-intensity diffraction peaks at 25.1°, 38.1°, 47.9°, 54.2°, 55.0° and 62.7° were present at the XRD spectra of FTG, BT and BTC (Fig. 2a), which were classified to the (101), (004), (200), (105), (211) and (204) crystal plane structure of TiO_2 according to the standard FDF #21-1272 spectra [41,42]. However, a significant sharp peak at 25.1° and multiple broad peaks (29.6°–33.1°, 39.1°, 45.5° and 49.2°) were observed in FT, which were ascribed to (101) crystal plane of TiO_2 and amorphous form of organic Ti compounds (such as $Ti_6O_6(Ac)_6(OBu)_6$) [41,42], respectively. Fourier transform infrared spectroscopy (FTIR) spectra of FT also confirmed the existence of these organic components for the multiple strong vibration at 500–1000 cm^{-1} (Fig. 2b). These results suggested that the organic Ti component in FTG, BT and BTC had been transformed into anatase type structure after annealing treatment. Moreover, FTG had a similar XRD spectrum to commercial P25, but the intensity of characteristic peak was weakened due to the intervention of graphene. The peaks located at the 62.7°, 68.9°, 70.4° and 74.9°, classified as (204), (116), (220) and (215) crystal planes, had almost been eliminated in BT and BTC, which was attributed to the reduction effect of sodium borohydride and the entanglement and covering effect of CNT to TiO_2 particle [43]. FTIR results (Fig. 2b) showed that the number of vibration peaks in FTG, BT and BTC was significantly decreased compared to FT. Specifically, multiple Ti–O (780 cm^{-1}) or Ti–O–C (819.2 cm^{-1}) vibration peaks for FT were replaced by a large broad vibration peak for FTG, BT and BTC when the wave number was less than 1000 cm^{-1}. This was ascribed to decomposition and elimination of impurity components during annealing treatment [44,45], which was consistent with the XRD results. Additional C=C/C=O (1596 cm^{-1}), Ti–OH (1343 cm^{-1}), TiO_2–B (895 cm^{-1}) and Ti–O–Ti (724 cm^{-1}) vibrational peaks were observed in BT and BTC. These O rich functional groups could be provided more active sites to bind ABFP coatings or produce active species. Meanwhile, the Ti containing groups on surface of FTG and BTC was blocked by additional graphene or CNT, and present several weak C=C/C=O or Ti–O–C vibration peaks in FTG and BTC. And both FTG and BTC had more Ti containing groups compared with pure graphene or CNT (Fig. S5 in Supporting information). These above results indicated that graphene or CNT was undergoes recombination and binding with TiO_2 particle surface as carbon bridge, rather than simple adsorption.

The X-ray photoelectron spectroscopy (XPS) whole spectra revealed that the Ti, O or C elements was the main components on FT, FTG, BT and BTC surface (Fig. S6a in Supporting information). The proportion of Ti^{3+} in BTC was significantly higher than that in FTG and pure TiO_2 (Fig. S6b in Supporting information), which was ascribed to the oxygen enrichment treatment ($NaBH_4$) reduced partly Ti^{4+} to Ti^{3+} and formed O_v (oxygen vacancies) [46]. These O_v sites could play as active sites for the binding of CNT or ABFP and generate photocatalytic activity [47]. The XPS spectra of O 1s for FTG and BTC was deconvoluted into Ti–O (lattice oxygen species) and defective oxygen (O^{2-}, C–O or C=O) at 531.15 eV and 532.05 eV, respectively (Fig. 2c). An additional -OH peak was recognized at 535.70 eV, which was usually considered as H_2O molecules adsorbed on the BTC surface [47]. These heterogeneous defect oxygen sites could regulate the d-band center of TiO_2 and contribute to the generation of reactive species [48]. It could be inferred that BTC had better adsorption or reactivity for water, while the single TiO_2 was lack of active sites due to the lower proportion of defective oxygen (Figs. S7 and S8 in Supporting information). Additionally, the C 1s spectra of BTC and FTG was deconvoluted into C=C/C–C, C–O/C–Ti and C=O, located at 284.50 eV, 285.40/284.9 eV and 288.25 eV, respectively (Fig. 2d). These results were demonstrating the binding effects between C and Ti components, and confirmed that the introduction of CNT or graphene was provide the additional active sites (such as C=C, C=O and C–O) on the surface of TiO_2 particle, which was conducive to the transfer of photoelectrons *via* the carbon bridge.

Inspired by the unique carbon bridge effect between TiO_2 particle and ABFP of FTG and BTC, the antibacterial performance of FTP, FTGP, BTP and BTCP coatings to *S. aureus* and *E. coli* in artificial seawater were conducted (Fig. 3). Compared to the blank group (glass) and control group (ABFP), the growth and reproduction of *S. aureus* and *E. coli* on different FTP, FTGP, BTP and BTCP coating surfaces had been significant inhibited (Fig. 3a). Specifically, the antibacterial rates to *S. aureus* and *E. coli* were 50.96% and 52.65% for single ABFP coating. This indicated that solely relying on the polymers surface of ABFP was difficult to resist the bacterial erosion. Nevertheless, the antibacterial rates of FTP, FTGP, BTP and BTCP for *S. aureus* were significantly improved to 81.83%, 88.34%, 84.83% and 89.33%, respectively, and the antibacterial rates for *E. coli* were 93.60%, 98.21%, 94.50% and 96.70% (Figs. 3b and c). The antibacterial rate of composite coatings was over 1.64-fold (for *S. aureus*) and 1.74-fold (for *E. coli*) more than that of single ABFP coatings. Obviously, this might be attributed to the introduction of photocatalysts (FT, FTG, BT, BTC) changed the antibacterial pathway and improved the antibacterial efficiency of ABFP coating by the

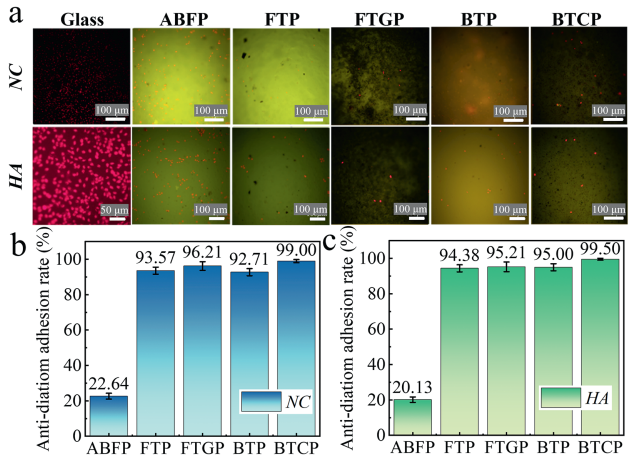

Fig. 4. (a) Diatom adhesion fluorescence microscopy images and (b and c) the anti-diatom adhesion ability for different coatings.

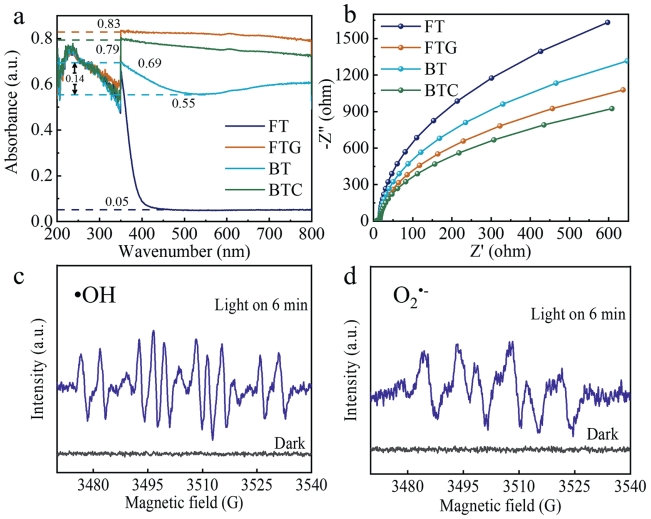

Fig. 5. The (a) UV–vis DRS, (b) EIS of FT, FTG, BT and BTC; electron spin resonance (ESR) spectra signals of (c) ·OH and (d) $O_2^{\bullet-}$ on BTCP-water or methanol system with or without light.

photocatalyst reaction. FTGP and BTCP showed a higher antibacterial efficiency than that of FTP and BTP in both *S. aureus* and *E. coli* system, which might be attributed to the enhanced photocatalytic ability of FTGP and BTCP by graphene and CNT addition. Moreover, all tested coatings showed a better antibacterial rate to *E. coli* than *S. aureus*. It had been reported that *S. aureus*, as a typical gram-positive bacterium, had a thicker cell wall for the abundant peptidoglycan and teichoic acids than *E. coli* [49,50], which explained the uneasy breakage of *S. aureus* cell wall after being attacked by photocatalytic reactions and active species.

Coatings with different FT, FTG, BT or BTC additional dosage showed over 90% antibacterial rates to both *S. aureus* and *E. coli* (Fig. S9 in Supporting information). Excessive photocatalyst addition dosage (>5 wt%) could increase the roughness of the ABFP coating, which provided more breeding sites for bacteria [10]. Moreover, excessive addition of graphene or CNT might block the active sites of TiO_2 particles or increase photoelectron transmission distance (Figs. 1b–e), and inhibiting its photocatalytic ability. Therefore, 3 wt% graphene and CNT was recommended addition dosage for FTGP and BTCP.

In addition, *NC* and *HA* were selected as representative algae to test anti-diatom adhesion ability of prepared coatings. The fluorescence microscopy images of *NC* and *HA* were shown in Fig. 4a, and significantly inhibited effect was observed in *NC* and *HA* with FTP, FTGP, BTP and BTCP coatings. *NC* and *HA* had achieved rapid growth in glass group and fluorescent dots (red) fill the entire image (Fig. 4a glass), while it was decreased by 22.15% and 20.38% in single ABFP within 24 h, respectively (Figs. 4b and c). BTCP showed the best anti-diatom adhesion rate in both *NC* (99.00%) and *HA* (99.50%) system (Figs. 4b and c). Meanwhile, the anti-algae efficiency of all prepared coatings was slightly higher than that of antibacterial efficiency because of size differences between algae and bacteria. The photocatalyst addition dosage result shown that there was an optimal addition dosage for FT, FTG, BT and BTC, excessive addition was not conducive to improve the anti-diatom adhesion ability of corresponding coatings (Fig. S10 in Supporting information). Excessive addition of carbon materials (graphene or CNT) not only increased the roughness of the coating, but also covered the active sites on the surface of TiO_2. The antifouling performance of FTGP or BTCP was significantly better than some reported studies (Table S1 in Supporting information). In brief, BTCP with 3 wt% BTC addition were recommended coatings and had the best anti-diatom adhesion efficiency (>99.00%).

In order to reveal the role of graphene or CNT in TiO_2-ABFP coatings, the ultraviolet–visible diffuse reflection spectrum (UV–vis DRS), energy bandgap, electrochemical impedance spectroscopy (EIS) and *i-t* curve were conducted and present in Fig. 5. UV–vis DRS spectra revealed that the order of light absorption intensity was FT < BT < BTC < FTG for the whole wavenumber (200–800 nm) (Fig. 5a). In other words, FTG might had the best light utilization efficiency in whole wavenumber due to the excellent structure and light absorption efficiency of graphene. Similar results had also been observed in other literatures, typically associated with graphene regulating the lattice of TiO_2 [40,51]. Moreover, a significant difference occurred in wavelength range of visible light (350–800 nm), the visible light absorption of FTG and BTC had been significantly improved and stabilized at 0.79–0.83 a.u., while a sharp decreases and stabilizes at 0.05 a.u. trends were observed for FT. And an unstable absorbance trend (sharp rise followed by slow decline and gradual rise until equilibrium) and lower intensity (0.55–0.79 a.u.) was observed in BT with the wavelength increased from 350 nm to 800 nm. This indicated that the addition of graphene or CNT could improve the visible light absorption performance of TiO_2, while the effect of sodium borohydride modification was unstable. The effect of addition dosage results further showed that excessive or insufficient addition of CNT or graphene was not conducive to improve the catalyst's absorption of visible light, which consistent with the public reports [51,52], and BTC-3% and FTG-3% achieved the optimal activity for visible light (Fig. S11 in Supporting information). Therefore, an appropriate additional proportion (3 wt%) of graphene or CNT in TiO_2 particle might be the key factor to improving the antifouling performance of FTGP and BTCP due to its wider absorption range for light.

The energy bandgap of FT, FTG, BT and BTC were 3.07 eV, 1.63 eV, 1.78 eV and 1.97 eV, respectively (Fig. S12a in Supporting information). Lower energy bandgap represents a less energy from light was needed to activate electron transfer in FTG or BTC, which also means a better utilization efficiency of sunlight and lead to a well photocatalytic potential. Literatures had been pointed out that lower bandgap indicated higher mobility of valence electrons in TiO_2 lattice, which might improve the conductivity of the TiO_2 [31,52]. These results confirmed that FTG and BTC had better photocatalytic efficiency, which in turn promoted the corresponding antifouling performance of FTGP and BTCP.

Furthermore, the ESI curves were measured and showed in Fig. 5b. A significantly increase of -Z" for FT, FTG, BT and BTC was observed when Z' continuously increasing (>20 ohm), and BTC had

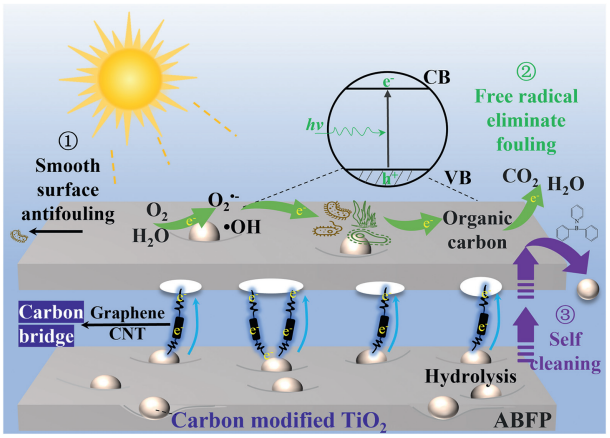

Fig. 6. Proposed mechanism of antifouling by FTGP or BTCP in seawater.

the lowest -Z" values in the medium-frequency region. This indicated that BTC could maintain better conductivity under lower applied voltage due to the additional CNT improve the electron transfer efficiency in TiO_2. FTG also had significantly lower resistance than BT and FT. In addition, due to higher photocurrent response values under the same light stimulation in the photocurrent-time curves (Fig. S12d in Supporting information), which revealed FTG and BTC were more sensitive to electron migration [52,53]. This indicated that CNT presented better improvement of TiO_2 conductivity than that of graphene. Therefore, since graphene or CNT was binding on TiO_2 surface with C-Ti/Ti-O (Figs. 2c and d), it could be concluded that the additional graphene or CNT might plays a bridging role in the process of photoelectron generation and transfer, thereby improving the antifouling ability of FTGP or BTCP.

Obvious signals of hydroxyl (•OH) and superoxide radicals ($O_2^{\bullet-}$) were detected for BTCP with light on 6 min, while not detected in dark condition (Figs. 5c and d). This result confirmed the electron transfer bridging effect of CNT and revealed that BTCP could rapidly generate large number of reactive oxygen species (ROS, •OH and $O_2^{\bullet-}$) through CNT mediation, thereby inhibiting the growth of algae and bacteria on the coating surface.

Both graphene and CNT could improve the structure, light absorption, and photoelectric conversion effect of TiO_2, which were the key for the better antifouling performance of BTCP or FTGP. We further summarized the generic antifouling mechanism of FTGP and BTCP in seawater with light, which was presented in Fig. 6. Firstly, graphene and CNT provided more functional groups and played as a "link" or bridge between the interface of TiO_2 and ABFP, which formed a smoother coating surface and reduced the accessibility of pollutants or organism. Secondly, both FTGP and BTCP acquired extra photocatalytic pathway on antifouling due to the wider light absorption range and more sensitive photoelectric effect of FTG and BTC particles. Specifically, the FTG or BTC particles which embedded in ABFP coating could be activated to generate abundant holes and release electrons on TiO_2 under both ultraviolet and visible light. During this electron transfer process, graphene, or CNT in FTGP or BTCP acted as electron bridges, rapidly and smoothly transferred electrons to the coating surface. And then the activated electron and holes further reacted with water molecules or dissolved oxygen to rapidly produce •OH and $O_2^{\bullet-}$. These radicals with high oxidation capacity could effectively destroy the DNA or proteins in algae or bacterial cells, thereby prevented their adhesion and growth on the coating surface. In addition, both FTGP and BTCP also had self-cleaning properties because of the slow hydrolysis reaction of ABFP coatings [21]. The hydrolysis products had been confirmed by the detection of acetophenone, dimethylbenzyl alcohol, pyridine, formic acid, or boronbenzenes groups (Table S2 in Supporting information). In other words, this self-cleaning property not only removed stubborn biological residues or inorganic impurities, but also exposed and replaced of the photocatalytic active surface of new FTG or BTC to maintain efficient generation of ROS (•OH and $O_2^{\bullet-}$). The hydrolysis products generated through self-cleaning processes were further decomposed into CO_2 and H_2O under the action of visible light and ROS. Additionally, BTCP or FTGP also exhibits good stability (Fig. S13 in Supporting information) and environmental friendliness (Fig. S14 in Supporting information). Photocatalytic processes on composite coatings surface could degrade the hydrolysis products of ABFP, which reduced the toxic of ABFP coatings to the environment and organisms. Therefore, FTGP and BTCP provided a feasible perspective and approach to unify the efficient performance and environmental friendliness of antifouling coatings.

In summary, we developed serials photocatalyst and composite antifouling coatings with raw material of graphene or CNT, TiO_2 and ABFP *via* hydrothermal and annealing treatment. The introduction of graphene and CNT had brought new functional groups (C–O, C–Ti–O, *etc.*) and spatial structures (petal gaps, entanglement) to TiO_2 particle, which also played a "link" or bridge role in the combination process of TiO_2 and ABFP, and significantly improved tightness and smoothness of the composite antifouling coatings of FTGP and BTCP. BTCP showed the best antibacterial (89.33%) and anti-diatom adhesion rate (99.50%), which were 1.84-fold and 4.94-fold that of single ABFP. The recommended additional ratio was 3 wt% of graphene or CNT to TiO_2 and 5 wt% of TiO_2 to ABFP. Proper addition of graphene or CNT significantly enhances photocatalytic activity of TiO_2 and improves the transfer efficiency of active species between coatings. Carbon bridge effect between TiO_2 and ABFP enhance the synergies antifouling process. More attempts are needed to explore the modification effects of other engineering carbon materials (activated carbon, biochar) on TiO_2 in the future. Our work provides a new insight into the regulation of TiO_2 and the antifouling mechanism of polymer coating.

Declaration of competing interest

The authors declare that there are no completing interests.

CRediT authorship contribution statement

Jiatong Li: Conceptualization, Formal analysis, Investigation, Writing – original draft. **Linlin Zhang:** Data curation, Funding acquisition, Methodology, Resources. **Peng Huang:** Funding acquisition, Methodology, Supervision, Writing – review & editing. **Chengjun Ge:** Funding acquisition, Project administration, Supervision.

Acknowledgments

This work was supported by the National Natural Science Foundation of China (Nos. 42277315, 22066009) and the Scientific Research Startup Fund of Hainan University (Nos. XJ2300005916, kyqd (zr) 22185); this work was also supported by Scientific Research Project of Hainan Higher Education Institutions (No. Hnky2023-9) and Innovational Fund for Scientific and Technological Personnel of Hainan Province (No. KJRC2023C12).

Supplementary materials

Supplementary material associated with this article can be found, in the online version, at doi:10.1016/j.cclet.2024.109970.

References

[1] S. Cao, J. Wang, H. Chen, D. Chen, Chin. Sci. Bull. 56 (2011) 598–612.
[2] H. Jin, L. Tian, W. Bing, et al., Prog. Mater. Sci. 124 (2022) 100889.
[3] M.S. Selim, M.A. Shenashen, S.A. El Safty, et al., Prog. Mater. Sci. 87 (2017) 1–32.
[4] H. Qiu, K. Feng, A. Gapeeva, et al., Prog. Polym. Sci. 127 (2022) 101516.
[5] M.R.N. Lee, U.J. Kim, I.S. Lee, et al., Mar. Pollut. Bull. 99 (2015) 157–165.
[6] M. Lagerström, J. Strand, B. Eklund, E. Ytreberg, Environ. Pollut. 220 (2017) 1333–1341.
[7] J.F. Marchand, Science 104 (1946) 74–75.
[8] M. Zhai, Y. Gong, X. Chen, et al., Surf. Coat. Technol. 328 (2017) 115–120.
[9] A.P. Ferris, I. McDermott, Nature 212 (1966) 284–285.
[10] S. Pourhashem, A. Seif, F. Saba, et al., J. Mater. Sci. Technol. 118 (2022) 73–113.
[11] Z. Li, P. Liu, S. Chen, et al., Eur. Polym. J. 190 (2023) 111997.
[12] Y. Wu, W. She, D. Shi, et al., Compos. Part B 195 (2020) 108031.
[13] M. Cui, X. Chen, S. Mei, S. Ren, Chem. Eng. J. 471 (2023) 144760.
[14] H. Zhang, Y. Li, S. Tian, et al., Chem. Eng. J. 436 (2022) 135072.
[15] Z. Zhang, R. Chen, J. Yu, et al., Chem. Eng. J. 474 (2023) 145540.
[16] H. Zheng, L. Liu, F. Meng, et al., J. Mater. Sci. Technol. 84 (2021) 86–96.
[17] S. Dolui, D. Kumar, S. Banerjee, B. Ameduri, Acc. Mater. Res. 2 (2021) 242–251.
[18] A.M.C. Maan, A.H. Hofman, W.M. de Vos, M. Kamperman, Adv. Funct. Mater. 30 (2020) 2000936.
[19] P. Wang, B. He, B. Wang, et al., Prog. Org. Coat. 165 (2022) 106706.
[20] Y. Li, R. Chen, Y. Feng, et al., Ind. Eng. Chem. Res. 58 (2019) 8016–8025.
[21] X. Sun, L. Zhang, R. Chen, et al., J. Colloid Interface Sci. 608 (2022) 1802–1812.
[22] Y. Li, R. Chen, L. Zhang, et al., Colloids Surf. A 582 (2019) 123865.
[23] Z. Yu, X. Li, X. Li, et al., Adv. Funct. Mater. 33 (2023) 2305995.
[24] Y. Gu, L. Yu, J. Mou, et al., Mar. Drugs 18 (2020) 1–22.
[25] L. Zhang, J. Sha, R. Chen, et al., J. Hazard. Mater. 389 (2020) 121854.
[26] S. Sinha, R. Kumar, J. Anand, et al., ACS Appl. Nano Mater. 6 (2023) 12828–12848.
[27] J.Y. Park, Science 361 (2018) 753.
[28] N. Rahimi, R.A. Pax, E.M. Gray, Prog. Solid State Chem. 44 (2016) 86–105.
[29] S. Selcuk, X. Zhao, A. Selloni, Nat. Mater. 17 (2018) 923–928.
[30] F. Xu, K. Meng, B. Cheng, et al., Nat. Commun. 11 (2020) 4613.
[31] Y. Liu, L. Tian, X. Tan, et al., Sci. Bull. 62 (2017) 431–441.
[32] S. Liang, X. Wang, Y.J. Cheng, et al., Energy Storage Mater. 45 (2022) 201–264.
[33] J. Arun, S. Nachiappan, G. Rangarajan, et al., Environ. Chem. Lett. 21 (2023) 339–362.
[34] Y. Liang, G. Huang, X. Xin, et al., J. Mater. Sci. Technol. 112 (2022) 239–262.
[35] V. Rodríguez González, C. Terashima, A. Fujishima, J. Photochem. Photobiol. C 40 (2019) 49–67.
[36] T.D. Nguyen Phan, V.H. Pham, E.W. Shin, et al., Chem. Eng. J. 170 (2011) 226–232.
[37] W. Yu, B. Zheng, K. Mao, et al., J. Cleaner Prod. 361 (2022) 132261.
[38] Á.T. Moranchel, A. Manassero, M.L. Satuf, et al., Appl. Catal. B 246 (2019) 1–11.
[39] J. Dustebek, C. Kandemir Cavas, S.F. Nitodas, L. Cavas, Prog. Org. Coat. 98 (2016) 18–27.
[40] M.R.F. Silva, M.A.O. Lourenço, D.M. Tobaldi, et al., Chem. Eng. J. 387 (2020) 124099.
[41] C. Wang, X. Cai, Y. Chen, et al., Chem. Eng. J. 317 (2017) 522–532.
[42] A. Sharma, P. Negi, R.J. Konwar, et al., J. Mater. Sci. Technol. 111 (2022) 287–297.
[43] X. Tian, M. Zahid, W. Sun, Y. Zhu, Appl. Surf. Sci. 566 (2021) 150615.
[44] L. Bi, Z. Chen, L. Li, et al., J. Hazard. Mater. 407 (2021) 124759.
[45] H. Zhao, W. Han, Z. Tang, Appl. Catal. B 276 (2020) 119133.
[46] T.W. Kim, M. Park, H.Y. Kim, S.J. Park, J. Solid State Chem. 239 (2016) 91–98.
[47] Z. Song, J. Hrbek, R. Osgood, Nano Lett. 5 (2005) 1327–1332.
[48] S. Zhang, R. Wang, K. Wang, et al., Environ. Sci. Technol. 58 (2024) 1921–1933.
[49] Z. Liu, M. Huang, A. Li, H. Yang, Water Res. 119 (2017) 57–66.
[50] G. Guan, L. Zhang, J. Zhu, et al., J. Hazard. Mater. 402 (2021) 123542.
[51] M. Minella, F. Sordello, C. Minero, Catal. Today 281 (2017) 29–37.
[52] A. Meng, L. Zhang, B. Cheng, J. Yu, Adv. Mater. 31 (2019) 1807660.
[53] M. Fan, Z. Lin, P. Zhang, et al., Adv. Energy Mater. 11 (2021) 2003037.